Poultry Science®

MicroRNA-129-1-3p attenuates autophagy-dependent cell death by targeting MCU in granulosa cells of laying hens under H_2O_2-induced oxidative stress

Mingkun Zhu,[*,†] Ming Yan,[*,†] Jianfei Chen,[*,†] Huaiyu Li,[‡] and Yeshun Zhang[*,†,1]

[*]*School of Biotechnology, Jiangsu University of Science and Technology, Zhenjiang 212100, China;* [†]*Sericultural Research Institute, Chinese Academy of Agricultural Sciences, Zhenjiang 212100, China; and* [‡]*Qingdao Animal Husbandry Workstation (Qingdao Institute of Animal Science and Veterinary Medicine), Qingdao, Shandong 266100, China*

ABSTRACT The present study aimed to investigate the mechanism of microRNA-129-1-3p (**miR-129-1-3p**) in regulating hydrogen peroxide ($\mathbf{H_2O_2}$)-induced autophagic death of chicken granulosa cell by targeting mitochondrial calcium uniporter (**MCU**). The results indicated that the exposure of hens' ovaries to H_2O_2 resulted in a significant elevation in reactive oxygen species (**ROS**) levels, as well as the apoptosis of granulosa cells and follicular atresia. This was accompanied by an upregulation of glucose-regulated protein 75 (**GRP75**), voltage-dependent anion-selective channel 1 (**VDAC1**), MCU, mitochondria fission factor (**MFF**), microtubule-associated protein 1 light chain 3 (**LC3**) I, and LC3II expression, and a downregulation of peroxisome proliferator-activated receptor gamma coactivator-1 alpha (**PGC-1α**) and mitofusin-2 (**MFN2**) expression. In hens' granulosa cells, a luciferase reporter assay confirmed that miR-129-1-3p directly regulates MCU. The induction of oxidative stress through H_2O_2 resulted in the activation of the permeability transition pore, an overload of calcium, depolarization of the mitochondrial membrane potential, dysfunction of mitochondria-associated endoplasmic reticulum membranes (**MAMs**), and ultimately, autophagic cell death. The overexpression of miR-129-1-3p effectively mitigated these H_2O_2-induced changes. Furthermore, miR-129-1-3p overexpression in granulosa cells prevented the alterations induced by H_2O_2 in the expression of key proteins that play crucial roles in maintaining the integrity of MAMs and regulating autophagy, such as GRP75, VDAC1, MFN2, PTEN-induced kinase 1 (**Pink1**), and parkin RBR E3 ubiquitin-protein ligase (**Parkin**). Together, these in vitro- and in vivo-based experiments suggest that miR-129-1-3p protects granulosa cells from oxidative stress-induced autophagic cell death by downregulating the MCU-mediated mitochondrial autophagy. miR-129-1-3p/MCU calcium signaling pathway may act as a new target to alleviate follicular atresia caused by oxidative stress in laying hens.

Key words: microRNA-129-1-3p, MCU, oxidative stress, granulosa cell autophagy, laying hens

2023 Poultry Science 102:103006
https://doi.org/10.1016/j.psj.2023.103006

INTRODUCTION

During the process of mammalian ovarian follicle development, follicular atresia plays a crucial role as a selective mechanism (Matsuda et al., 2012), believed to be associated with apoptosis-induced granulosa cell death (Matsuda-Minehata et al., 2006). Nevertheless, recent research has increasingly indicated that the autophagic death of granulosa cells may also serve as a significant process in oxidative stress-induced follicular atresia, which acts independently or simultaneously with apoptosis (Shen et al., 2017; Yadav et al., 2019). Choi et al. reported that autophagy occurs primarily in the granulosa cells and promotes apoptotic cell death (Choi et al., 2010, 2011). For laying hens, with the increase of intensification degree, oxidative stress caused by egg production or other environmental factors (heat stress, heavy metals, mycotoxins, etc.) is an important reason for inducing granulosa cell death and thus follicular atresia (Wang and Zhang, 2021). Therefore, reducing the autophagy death of follicular granulosa cells of laying hens is a key technique to prevent follicular atresia induced by oxidative stress, thus extending the laying cycle and improving the laying rate.

Calcium ion ($\mathbf{Ca^{2+}}$) functions as a second messenger and plays an important role in the regulation of mitophagy and apoptosis. Under the stimulation of harmful factors such as hypoxia and hydrogen peroxide ($\mathbf{H_2O_2}$),

Received May 12, 2023.
Accepted July 31, 2023.

[1]Corresponding author: zyssri@just.edu.cn

calcium overload is a significant contributing factor to the initiation of autophagy (Kim et al., 2020). Ca^{2+} homeostasis is mainly regulated by membrane Ca^{2+} channels and intracellular Ca^{2+} stores, which encompass endoplasmic reticulum (**ER**), mitochondria, lysosomes, endosomes, and Golgi apparatus (Michelangeli et al., 2005). Among these, the mitochondrial-associated ER membranes (**MAMs**) plays a crucial role in maintaining intracellular Ca^{2+} homeostasis by facilitating the transportation of Ca^{2+} from the ER to mitochondria (Filadi et al., 2017). The mitochondrial calcium uniporter (**MCU**), located in the inner mitochondrial membrane, directly interacts with voltage-dependent anion-selective channel 1 (**VDAC1**) and controls Ca^{2+} flux across the mitochondrial membrane to maintain mitochondrial Ca^{2+} homeostasis under physiological conditions (De Stefani et al., 2015). However, under pathological conditions, MCU-mediated mitochondrial Ca^{2+} overload leads to reactive oxygen species (**ROS**) accumulation, mitochondria dysfunction, ATP depleted, and apoptosis (Peng and Jou, 2010). Studies indicated that knockdown of MCU results in a reduction of mitochondrial Ca^{2+} uptake in response to histamine stimulation and mitigates cell death induced by oxidative stress (Cui et al., 2019). The MCU-VDAC1 complex may play an important role in regulating mitochondrial Ca^{2+} uptake and oxidative stress-induced apoptosis, rendering it a promising therapeutic target for diseases associated with oxidative stress (Liao et al., 2015). Therefore, the cell fate can be influenced by inhibiting or enhancing MCU levels to regulate the cellular calcium signaling.

MicroRNA (**miRNA**) is a noncoding RNA molecule ranging from 18 to 24 nucleotides in length. Its primary function is the negative regulation of gene expression, achieved through the suppression of mRNA translation or destabilization of mRNA molecules (Jovanovic and Hengartner, 2006; Jiang et al., 2020). MiRNAs are considered to regulate numerous protein-coding genes and various biological processes, such as cell differentiation, proliferation, metastasis, and angiogenesis (Zhu et al., 2021). Additionally, certain nuclear-encoded miRNAs, including mir-129, miR-15a, miR-16-1, and miR-34a, have been shown to participate in the modulation of calcium signaling and mitochondrial function (Gao et al., 2010; Li et al., 2012; Tai et al., 2021). Studies have shown that miR-129-3p targeted MCU alleviated neuronal damage mediated by glucose fluctuation via a mitochondrial-dependent intrinsic apoptotic pathway (Wang et al., 2021). The overexpression of miR-129-1-3p has been found to inhibit the proliferation, invasion, migration, and calcium overload of mouse breast cancer cells, while also promoting apoptosis (Li et al., 2021). However, the specific role of miR-129-1-3p in regulating H_2O_2-induced damage to granulosa cells and the underlying mechanisms involved remain unknown.

Hence, the current investigation aimed to evaluate the impact of miR-129-1-3p on autophagic cell death in chicken granulosa cells by targeting MCU under conditions of oxidative stress, while also elucidating the underlying molecular mechanisms.

MATERIALS AND METHODS

Experimental Animals

The study was approved by the Ethics Committee of the Jiangsu University of Science and Technology (G2022SJ12). A total of twelve 38-wk-old Hyline gray laying hens, with similar body weight (**BW**), were obtained from a commercial layer chicken farm in Zhenjiang, China. These hens were randomly divided into 2 groups: basal diet group (control group) and H_2O_2 group (feeding basal diet + intraperitoneal injection of 10% H_2O_2 (2.96 mmol H_2O_2/kg BW) on the ninth day of the experiment). The experiment lasted for 14 d. The injection time and dosage of H_2O_2 are referred to the reports of Xing et al. (2021) and Yan et al. (2022). On the 15th day of the experiment, ovary samples were collected from all test chickens and stored at −80°C for the detection of molecular biological related to oxidative stress and ROS staining. Other ovary samples were fixed in 4% paraformaldehyde for hematoxylin and eosin (**H&E**) and terminal deoxynucleotidyl transferase-mediated dUTP-biotin nick end labeling (**TUNEL**) staining.

Hematoxylin and Eosin Staining

The paraformaldehyde-fixed ovarian tissues were trimmed, dehydrated with graded gradients of ethanol, transparented in xylene, and then embedded in wax after being immersed at 58°C for 1 h. Subsequently, the tissues were sectioned with a microtome to a thickness of 5 to 6 μm. Following dewaxing with xylene, hydrating with gradient alcohol concentrations, and staining with H&E, the sections were examined under an optical microscopy (400×, Olympus, Tokyo, Japan) to identify any histopathological findings.

TUNEL Assay

The apoptotic cells in the ovarian tissues of hens were detected through in situ analysis using TUNEL. The sections were mounted onto slides and coverslipped with 2-(4-amidinophenyl)-6-indolecarbamidine dihydrochloride (**DAPI**). Sections were then examined using a laser-scanning confocal microscope (Carl Zeiss).

Cell Isolation and Culture

Large white follicles (2−5 mm in diameter) of laying hens were collected under sterile conditions and immediately transferred to contain phosphate buffered saline (**PBS**) sterile petri dishes. The granular layers were separated and transferred to sterile 50 mL centrifuge tubes and digested in serum-free medium (DMEM/F12, 1:1) containing 1% type I collagenase (Solarbio, Beijing, China) at 37°C for 10 min. The digested cells were terminated by adding complete medium (DMEM/F12 containing 10% fetal bovine serum (10099141C, Gibco, Carlsbad, CA)) in equal proportions, filtered with 3

Table 1. Sequences of the miR-129-1-3p mimics, inhibitors and negative controls used in cell transfection.

Name	Sequence (5′−3′)
gga-miR-129-1-3p mimics	F: AAGCCCUUACCCCAAAAAGCAU R: GCUUUUUGGGGUAAGGGCUUUU
mimics NC	F: UUGUACUACACAAAAGUACUG R: GUACUUUUGUGUAGUACAAUU
gga-miR-129-1-3p inhibitor	(mA)(mU)(mG)(mC)(mU)(mU)(mU)(mU) (mU)(mG)(mG)(mG)(mG)(mU)(mA) (mA)(mG)(mG)(mG)(mC)(mU)(mU)
inhibitor NC	CAGUACUUUUGUGUAGUACAA

Abbreviations: F, forward; gga, gallus; NC, negative control; R, reverse.

layers of gauze, and centrifuged at 1,000 rpm for 5 min. After extensive washing with PBS, the cells were resuspended, and subsequently cultured in complete medium for 3 or 4 d at 37°C, 5% CO_2 for further processing.

Cell Transfection and H_2O_2 Treatment

H_2O_2 stock solution including 1 M H_2O_2 was prepared by dissolving hydrogen peroxide 30% aqueous solution (Sinopharm Chemical Reagent Co., Ltd., Shanghai, China) with sterile distilled water. After 4 d of culture, cells were treated with 0, 100, 200, 400, 600, 700, 800, and 1,000 μM H_2O_2 (1.8 μL of sterile distilled water without H_2O_2 was added to the control group). The miR-129-1-3p inhibitor, inhibitor negative control (inhibitor NC), miR-129-1-3p mimics and mimics negative control (mimics NC), shown in Table 1, were prepared by Sangon Biotech Co., Ltd. (Shanghai, China). As the manufacturer's instructions, the miRNAs were transfected into chicken granulosa cells for 12 h in complete medium using Hieff Trans Liposomal Transfection Reagent (Yeasen, Shanghai, China). Then, fresh complete medium was used to replace the medium containing transfection reagents and the culture was continued for 24 h. Cells were treated with H_2O_2 or collected to evaluate the transfection effect through measuring MCU expression level using Western blot method.

Cell Viability Assay

A 96-well plate was seeded with roughly 1×10^4 cells per well. Subsequently, the cells were subjected to various concentrations of H_2O_2 (0, 100, 200, 400, 600, 700, 800, and 1,000 μM) for a duration of 3 h. Following this treatment, the cells were incubated for an additional 2 h after adding 10 μL of Cell Counting Kit-8 (Sangon Biotech, Shanghai, China). The absorbance at 450 nm was measured with a fluorescence microplate reader (Bio-Tek, Highland Park, Winooski, VT).

ROS Analysis

Methods for the detection of ROS in ovarian tissue were performed based on the previous description (Zhu et al., 2020b). Fresh ovarian tissues (10 mm, 3 in each group) were embedded in Tissue-Tek optimal cutting temperature (**OCT**) embedding compound and sectioned into frozen sections with a thickness of 8 to 10 mm. Subsequently, a 200 mL solution of dihydroethidium (**DHE**) was topically applied to the ovarian sections, followed by a 30-min incubation at 37°C. Excess DHE was then rinsed off 3 times with PBS. Images were captured using an OLYMPUS fluorescent microscope (Tokyo, Japan) with excitation and emission wavelengths of 520 and 610 nm, respectively. All aforementioned procedures were conducted in a light-proof environment.

A 2,7-dichlorodihydrofluorescein diacetate (**DCFH-DA**) method was used to analyze ROS levels in granulosa cells. Cells were collected after treatment and incubated in serum-free DMEM/F12 containing 10 μmol/L DCFH-DA (Beyotime, Shanghai, China) at 37°C for 20 min. The blank controls omitted DCFH-DA incubation. The cells were immediately imaged using an OLYMPUS fluorescent microscope (Tokyo, Japan) or subjected to flow cytometry using a FACSverse flow cytometer (BD Biosciences, San Jose, CA) after being washed with serum-free DMEM/F12. Data were analyzed using FlowJo program based on the FL1 channel.

Total RNA Isolation and qRT-PCR

In accordance with the previously described methods, total RNA was extracted and quantitative real-time PCR (**qRT-PCR**) was performed (Zhu et al., 2020a). As shown in Table 2, qRT-PCR primer sequences are provided.

Western Blot Analysis

For the extraction of total cellular proteins, granulosa cells were lysed in lysis buffer. Four to 20% sodium dodecyl sulfate-polyacrylamide gel electrophoresis (**SDS-PAGE**) was used to load the proteins, followed by transfer onto PVDF membranes. The membranes were incubated with Beclin1 (dilution 1:1,000, catalog no. AP0768, Bioworld, Nanjing, China), microtubule-associated protein 1 light chain 3I/II (LC3I/II, dilution 1:3,000, catalog no. 14600-1-AP, Proteintech, Wuhan, China), parkin RBR E3 ubiquitin-protein ligase (**Parkin**, dilution 1:1,000, catalog no. A11172, Abclonal, Wuhan, China), PTEN-induced kinase 1 (**PINK1**, dilution 1:1,000, catalog no. A7131, Abclonal, Wuhan, China), inositol 1,4,5-trisphosphate receptor (**IP3R**, dilution 1:1,000, catalog no. A21471, Abclonal, Wuhan, China), glucose-regulated protein 75 (**GRP75**, dilution 1:1,000, catalog no. A11256, Abclonal, Wuhan, China), VDAC1 (dilution 1:3,000, catalog no. 55259-1-AP, Proteintech, Wuhan, China), mitofusin-2 (**MFN2**, dilution 1:5,000, catalog no. 12186-1-AP, Proteintech, Wuhan, China), MCU (dilution 1:1,000, catalog no. A16281, Abclonal, Wuhan, China), GAPDH and Tubulin β (dilution 1:5,000, as the loading control) antibodies at 4°C for 12 to 16 h. Then the membranes were incubated with secondary antibodies for 1 h at room temperature

Table 2. Primer used for quantitative real-time PCR.

Target gene	Primer	Primer sequence (5′−3′)	Accession no.
β-actin	Forward	TCCCTGGAGAAGAGCTATGAA	NM_205518.1
	Reverse	CAGGACTCCATACCCAAGAAAG	
Nrf2	Forward	CTGCCCAAAACTGCCGTA	NM_205117.1
	Reverse	TCAAATCTTGCTCCAGTTCCA	
Keap1	Forward	ACTTCGCTGAGGTCTCCAAG	MN416132.1
	Reverse	CAGTCGTACTGCACCCAGTT	
SOD1	Forward	TGTGCATGAATTTGGAGACAAC	NM_205064.1
	Reverse	TTGCAGTCACATTGCCGAG	
SOD2	Forward	TGCACTGAAATTCAATGGT	NM_204211.1
	Reverse	GTTTCTCCTTGAAGTTTGCG	
SOD3	Forward	TTTTCTCCTAAAGATGGCAAG	XM_420760.3
	Reverse	CTTCCTGCTCATGGATCACAA	
GST	Forward	GGAAGCCATTTTAATGACAGA	XM_046913335.1
	Reverse	TCCTTTAAAAGCCTGTAGCAGA	
GCLC	Forward	TCTGTAGATGATCGAACGC	XM_419910.4
	Reverse	TCCTTTATTAGGTGCTCGTAG	
GCLM	Forward	GCTGCTAACTCACAATGACC	NM_001007953.1
	Reverse	TGCATGATATAGCCTTTGGAC	
PGC-1α	Forward	TACAGCAATGAGCCTGCCAA	XM_046916274.1
	Reverse	AGGCAATCCATCCTCATCCAC	
Fis-1	Forward	TGTGTCCCTGTCTCCTTGT	XM_040657193.2
	Reverse	GTCACCACTGTGTCACCATATT	
MFF	Forward	ACTCAAAGTGGCTCCTCA	XM_040679333.2
	Reverse	CCTGCATAGTTACACTGG	
GRP75	Forward	AAGAGGCAGGCAGTAACTAATC	NM_001006147.2
	Reverse	CTTCAGACTTGTCCAGACCATAG	
VDAC1	Forward	GCCTGAAGCTGACTTTTGACTCC	XM_046927011.1
	Reverse	GATGTGCTCCCTTTTGTATCCTGT	
BNIP3	Forward	CATTACTTCATGCTGCGCCT	NM_001030885.3
	Reverse	CAAAGCAACCCAAGCCATCT	
LC3I	Forward	TTACACCCATATCAGATTCTTG	XM_040688401.2
	Reverse	ATTCCAACCTGTCCCTCA	
LC3II	Forward	AGTGAAGTGTAGCAGGATGA	NM_001031461.2
	Reverse	AAGCCTTGTGAACGAGAT	
MFN2	Forward	GACAGGTTGCCTTGTGAGATAG	XM_040689233.2
	Reverse	CCCATTCTTACCCTGGCATTAG	
MCU	Forward	TTGGCAGAGTGTGAGAGTGG	XM_046920626.1
	Reverse	AATTCCTCGGTCCTCTGCTT	
Caspase3	Forward	TCCCTGGTTCCAAAGGAATG	XM_015276122.2
	Reverse	AGTAGCCTGGAGCAGTAGAA	
Caspase8	Forward	CCCTGAAGACAGTGCCATTT	NM_204592.4
	Reverse	GGGTCGGCTGGTCATTTTAT	
miR-129-1-3p	Forward	CGAAGCCCTTACCCCAAA	
	Reverse	AGTGCAGGGTCCGAGGTATT	
U6	Forward	GGGCCATGCTAATCTTCTCTGTATCG	
	Reverse	GTGCAGGGTCCGAGGT	
RT-miR-129-1-3p	GTCGTATCCAGTGCAGGGTCCGAGGTATTCGCACTGGATACGACATGCTT		
RT-U6	GTCGTATCCAGTGCAGGGTCCGAGGTATTCGCACTGGATACGACCGATACA		

Abbreviations: BNIP3, Bcl-2 19-kDa interacting protein 3; Fis-1, fission 1; GCLC, glutamate-cysteine ligase catalytic subunit; GCLM, glutamate-cysteine ligase modifier subunit; GRP75, glucose-regulated protein 75; GST, glutathione-S-transferase; Keap1, kelch-like ECH-associated protein 1; LC3, microtubule-associated protein 1 light chain 3; MCU, mitochondrial calcium uniporter; MFF, mitochondria fission factor; MFN2, mitofusin-2; miR-129-1-3p, microRNA-129-1-3p; Nrf2, nuclear factor erythroid p45-related factor 2; PGC-1α, peroxisome proliferator-activated receptor gamma coactivator-1 alpha; SOD, superoxide dismutase; VDAC1, voltage-dependent anion-selective channel 1.

under the condition of avoiding light after fully washed with TBST buffer solution (1×). The chemiluminescence signal was detected by electrochemiluminescence (**ECL**, Yeasen, Shanghai, China) detection reagent. Blot bands were imaged using ChemiScope 6100 (Clinx Science Instruments Co., Ltd., Shanghai, China).

Dual-Luciferase Assay

The 3′-untranslated region (**3′-UTR**) of MCU was synthesized and inserted into the psiCHECK2.0 vector. The 3′-UTR of MCU (AAGGGCT), the possible miR-129-1-3p binding sites, was substituted with TCACTGA and validated via sequencing. The MCU-WT and MCU-MUT reporter plasmids were cotransfected into chicken granulosa cells with miR-129-1-3p mimic or NC mimic, respectively. The Dual Luciferase Reporter Assay kit (Yeasen, Shanghai, China) was used to perform luciferase assays. The Promega's Digital-Luciferase Reporter Assay System (Promega, Madison, WI) was used to detect dual-luciferase activity.

Determination of the Mitochondrial Membrane Potential

A fluorescent probe JC-1 (Beyotime, Shanghai, China) was used to detect the mitochondrial membrane potential (**MMP**). Briefly, the cells were incubated with JC-1 working buffer for 20 min, and images were

captured using OLYMPUS (Olympus Corporation, Tokyo, Japan). According to the manufacturer's protocol, a high level of MMP results in JC-1 aggregating in the matrix of the mitochondria to form polymers (J-aggregates) that produce red fluorescence. At low MMP levels, JC-1 cannot gather in mitochondria matrix and exists as a monomer that produce green fluorescence.

Transmission Electron Microscopy

Hens' granulosa cells were seeded in 6-well plates. Following treatment, the cells were fixed with a 2.5% glutaraldehyde solution at 4°C for 24 h. Subsequently, they were postfixed with 1% osmium tetroxide for 2 h, and subjected to gradient ethanol dehydration and epoxy resin embedding. The mitochondrial morphology was examined using a transmission electron microscope (JEM-1400, JEOL, Tokyo, Japan).

Mitochondrial Calcium Assay

Mitochondrial Ca^{2+} was examined using the fluorescent probe Rhod-2/AM (Yeasen, Shanghai, China) according to the manufacturer's guidance. Chicken follicle granulosa cells were washed with hanks balanced salt solution (without calcium and magnesium ions) for 3 times, and added with 4 μM Rhod-2/AM and incubated in darkroom for 30 min at 37°C. The cells were washed 3 times with probe-free buffer to adequately remove residual Rhod-2/AM working solution. Then buffer solution was added to cover the cells and incubated at 37°C for 30 min. All images were captured using a fluorescence microscope (OLYMPUS, Tokyo, Japan)

Mitochondria-Endoplasmic Reticulum Coupling Assay

Mitochondria and ER were examined using the fluorescent probe MitoTracker Green FM and ER-Tracker Red (BODIPY TR Glibenclamide) (Yeasen, Shanghai, China), respectively, according to the manufacturer's guidance. The culture solution was removed, the cells were cleaned with hank's balanced salt solution (**HBSS**) 3 times. The cells were incubated at 37°C for 20 min with preheated MitoTracker Green FM and ER-Tracker Red dyeing solution. After staining, the staining solution was replaced with fresh culture solution after washing 3 times with HBSS. All images were captured using a fluorescence microscope (OLYMPUS, Tokyo, Japan).

Statistical Analysis

The data were presented as the mean ± standard error of the mean (**SEM**) and analyzed using IBM SPSS Statistics 20.0. Multiple comparisons among groups were performed using 1-way ANOVA with Tukey's post hoc test ($P < 0.05$). Differences between 2 groups were determined by the unpaired t test ($P < 0.05$).

RESULTS

H_2O_2-Induced Oxidative Stress, Mitochondrial Dysfunction, Autophagy, Apoptosis, and Follicular Atresia in Ovary of Laying Hens

Results of H&E staining showed that hens exposed to H_2O_2 displayed more atretic follicles compared with control group (Figure 1A). To measure intracellular ROS in laying hen ovary tissues exposed to H_2O_2, an immunofluorescence assay was used. The result showed that the ROS level increased significantly in the H_2O_2 group (Figure 1B). As presented by the results of TUNEL assay, H_2O_2 exposure enhanced the granulosa cell apoptosis significantly ($P < 0.05$) (Figure 1C). Additionally, the mRNA expression levels of GRP75, VDAC1, MCU, mitochondria fission factor (**MFF**), LC3I, LC3II, and L3I/LC3II were observed to be upregulated, while the mRNA levels of peroxisome proliferator-activated receptor gamma coactivator-1 alpha (**PGC-1α**) and MFN2 were downregulated obviously in the H_2O_2 treatment group compared to the control group ($P < 0.05$) (Figure 1D). These findings confirm that H_2O_2 induces oxidative stress in the ovaries of laying hens, leading to mitochondrial dysfunction, autophagy, apoptosis, and ultimately follicular atresia.

H_2O_2-Induced Oxidative Stress in the Granulosa Cell of Laying Hens

Different concentrations of H_2O_2 (0, 100, 200, 400, 600, 700, 800, and 1,000 μM) were incubated with chicken granulosa cells to determine the consequences of increased oxidative stress on the cell viability. The results indicated that cell viability varied dose-dependently across all groups (Figure 2A). When compared to both the control and lower concentration groups, cell viability was significantly reduced in the groups exposed to higher concentration of H_2O_2 (700, 800, and 1,000 μM) ($P < 0.05$). 800 μM H_2O_2 increased the ROS production, and upregulated the expressions of kelch-like ECH-associated protein 1 (**Keap1**), superoxide dismutase 2 (**SOD2**), glutathione-S-transferase (**GST**), glutamate-cysteine ligase catalytic subunit (**GCLC**), glutamate-cysteine ligase modifier subunit (**GCLM**), MFF, LC3I, LC3II, Bcl-2 19-kDa interacting protein 3 (**bnip3**) and beclin1 genes or proteins, while concurrently downregulated the gene expressions of nuclear factor erythroid p45-related factor 2 (**Nrf2**), PGC-1α, and fission 1 (**Fis-1**) significantly (Figure 2B −D). Additionally, the administration of 800 μM H_2O_2 led to a significant loss of MMP compared to the control group (Figure 2E). Therefore, the most optimal and efficient concentration of H_2O_2 for inducing oxidative stress and autophagy was established to be 800 μM in our settings.

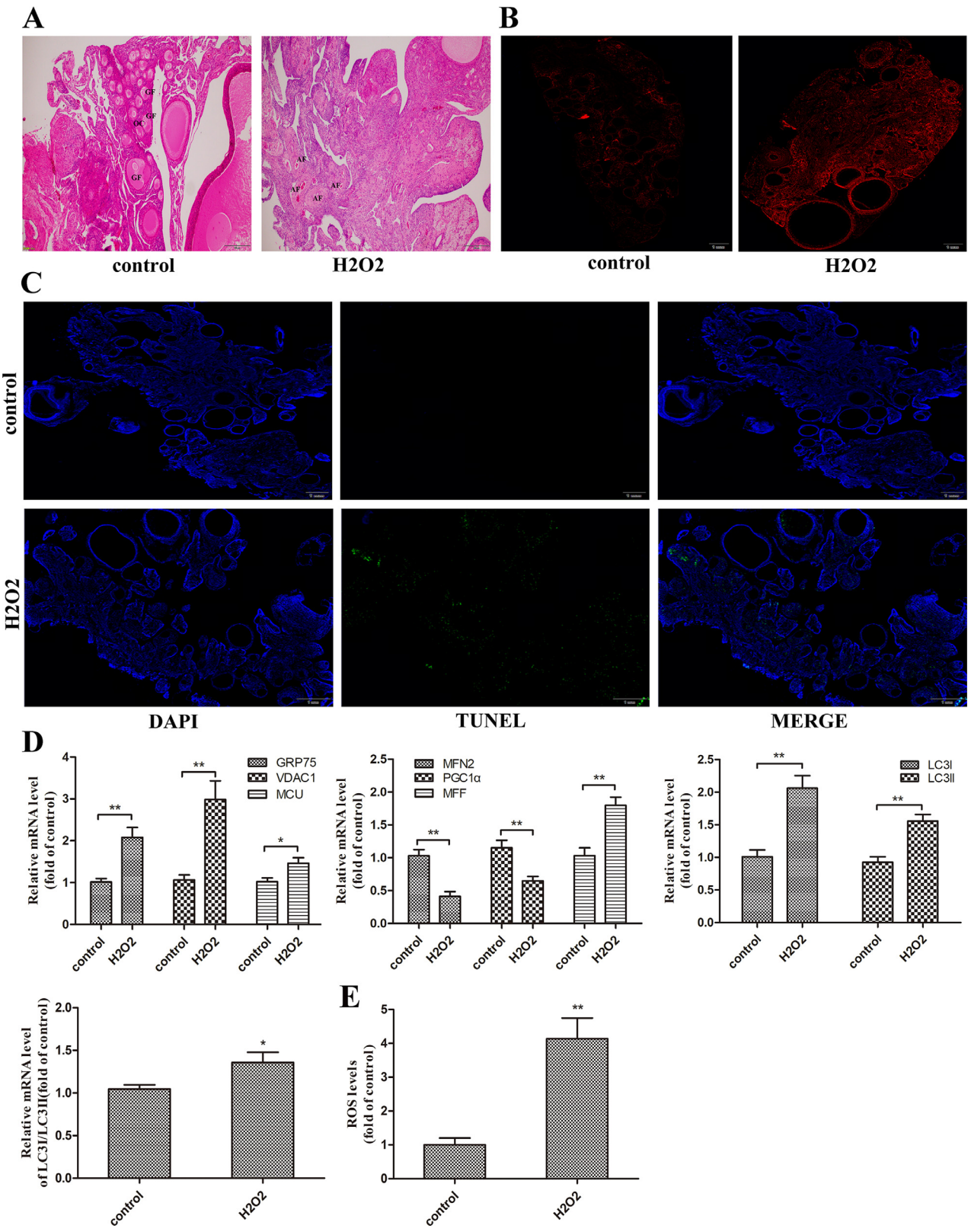

Figure 1. Hydrogen peroxide-induced oxidative stress, mitochondrial dysfunction, autophagy, apoptosis, and follicular atresia in ovary of laying hens. (A) The ovarian sections were stained with hematoxylin and eosin (scale bar = 200 μm). (B) ROS staining (scale bar = 1 mm). (C) Cell apoptosis (scale bar = 1 mm). (D) Quantification of mRNA levels-related mitochondrial function and autophagy. (E) Quantification of ROS levels in (B). Data are presented as mean ± standard error of the mean (SEM) ($n = 3$). Asterisks indicate significant differences ($^*P < 0.05$ and $^{**}P < 0.01$). Abbreviations: AF, atretic follicle; GF, growing follicle; OC, oocyte.

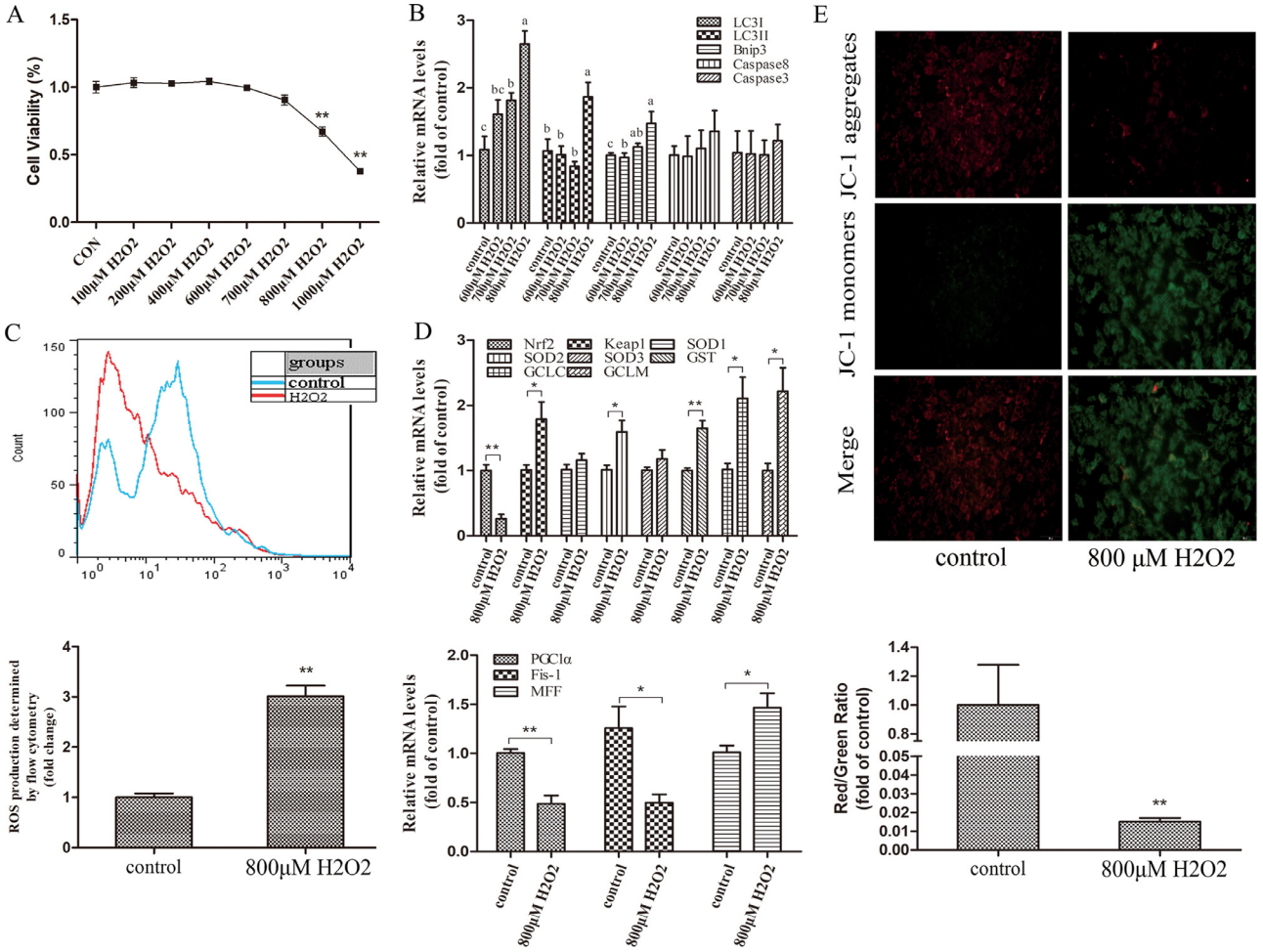

Figure 2. Hydrogen peroxide-induced oxidative damage, mitochondrial dysfunction and autophagy in chicken follicular granulosa cells. (A) Cell viability. (B) Apoptosis and autophagy-related gene Caspase 3, Caspase 8, LC3I, LC3II, and Bnip3 levels in granulosa cells. (C) ROS levels. (D) The expression of genes related to antioxidant and mitochondrial function. (E) Quantification of mitochondrial membrane potential ($\Delta\Psi$m) of granulosa cells by JC-1 aggregate monomer ratio. Data are expressed as mean ± SEM (standard error of the mean) ($n = 3$). There are significant differences between groups ($P < 0.05$) indicated by the different letters above the histogram (a–c). Asterisks indicate significant differences ($^*P < 0.05$ and $^{**}P < 0.01$).

H_2O_2 Activated the IP3R1-GRP75-VDAC1-MCU Complex in Granulosa Cells

As shown in Figure 3, when compared to control group, the administration of 800 μM H_2O_2 upregulated the expressions of IP3R, GRP75, VDAC1, MCU, beclin1, LC3I, and LC3II proteins significantly ($P < 0.05$).

Together, these data suggest that H_2O_2 activates the IP3R1-GRP75-VDAC1-MCU complex, leading to the promotion of oxidative stress and the induction of autophagy-dependent cell death in granulosa cells.

MiR-129-1-3p Directly Regulates MCU Expression in H_2O_2-Exposed Granulosa Cells

MiR-129-1-3p expression in chicken granulosa cells was markedly increased following oxidative stimulation (Figure 4A). As a further step toward elucidating regulatory mechanism of miR-129-1-3p in granulosa cells, we used microRNA target prediction database (**miRDB**) to predict the binding sites between miR-129-1-3p and MCU-3′ UTR (Figure 4C). A dual-luciferase assay was conducted to identify whether miR-129-1-3p directly targeted MCU. The result showed that overexpression of miR-129-1-3p obviously suppressed the relative luciferase activity of MCU with the WT 3′ UTR (**WT**) (Figure 4C). The results of qRT-PCR and Western blot showed that overexpression miR-129-1-3p inhibited the expression of MCU protein, which was upregulated through inhibition of miR-129-1-3p (miR-129-1-3p inhibitor) (Figure 4B and D). This confirmed that miR-129-1-3p mimics and inhibitor were successfully constructed and miR-129-1-3p could directly target MCU.

MiR-129-1-3p Overexpression Alleviates Autophagy in H_2O_2-Exposed Granulosa Cells by Targeting MCU

As shown in Figure 5, when compared to the group treated with 800 μM H_2O_2, miR-129-1-3p overexpression inhibited the expressions of MCU, beclin1, LC3I, and LC3II proteins significantly ($P < 0.05$) (Figure 5A). These findings, in conjunction with the observations made through transmission electron microscopy, demonstrate that miR-129-1-3p overexpression can effectively

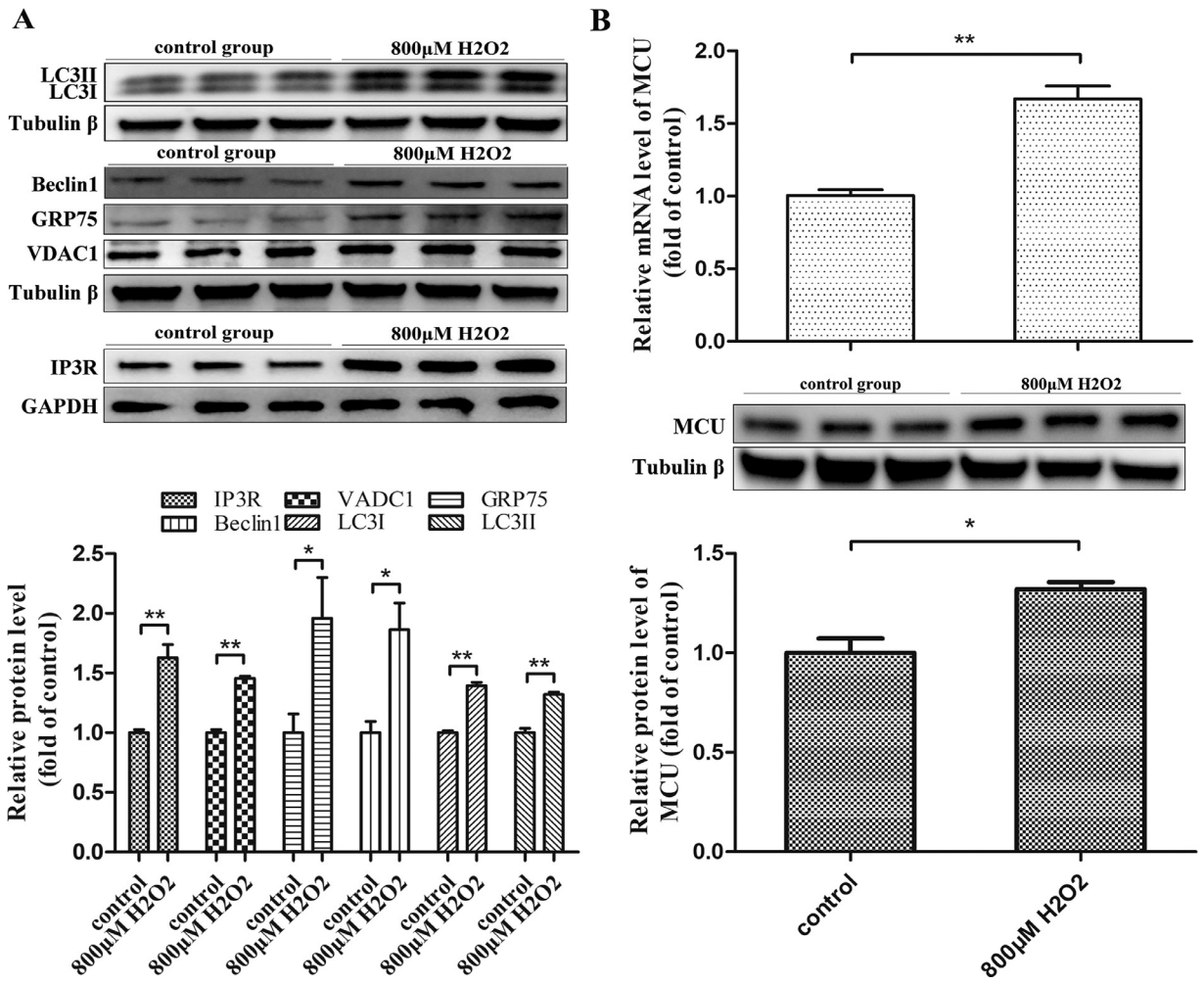

Figure 3. Effects of oxidative stress on the expression of MCU in granulosa cells of laying hens. (A) Western blot detection and quantification of IP3R, VDAC1, GRP75, Beclin 1, LC3I, and LC3II. (B) Real-time PCR and Western blot detection of MCU. Data are expressed as mean ± standard error of the mean (SEM) ($n = 3$). Asterisks indicate significant differences ($^*P < 0.05$ and $^{**}P < 0.01$).

mitigate the damage to mitochondria, and ER, as well as autophagy induced by H_2O_2 (Figure 5B).

MiR-129-1-3p Inhibits MCU Decreases ROS and Ca^{2+} Overload and Improves Mitochondria—ER Tethering

To further elucidate the molecular mechanism underlying the protective effect of miR-129-1-3p in follicular granulosa cells, we examined the effects of miR-129-1-3p overexpression on ROS and mitochondrial Ca^{2+} levels, MMP, MAMs integrity, and related proteins expression in granulosa cells. The results showed that miR-129-1-3p overexpression effectively inhibited the levels of ROS and mitochondrial Ca^{2+} (Figure 6A), as well as the disruption of MMP (Figure 6B) and mitochondria-ER tethering (Figures 6C and 5B) induced by exposure to H_2O_2 ($P < 0.05$). In addition, in comparison to the control group, H_2O_2 significantly increased pink1 and parkin proteins expression and decreased MFN2 protein expression. While, the expression of pink1 and parkin proteins were downregulated, and the expression of MFN2 protein was upregulated markedly in MCU siRNA group through overexpressing miR-129-1-3p (Figure 6D). These data suggest that miR-129-1-3p overexpression mitigates mitochondrial Ca^{2+} overload, ROS production, MMP depolarization, damage to mitochondrial-ER tethering, and initiation of mitophagy in granulosa cells.

DISCUSSION

Mounting evidence has suggested that autophagy and apoptosis are initiated simultaneously by the same stimulus (Saiki et al., 2011; Wei et al., 2014; Huang et al., 2016). A decreased scavenging or overproduction of ROS in response to environmental or metabolic factors leads to granulosa cell oxidative damage, which results in follicular atresia and relevant anovulatory disorders (Yang et al., 2019). Studies have demonstrated that ROS-mediated oxidative stress can induce autophagy in granulosa cells of mouse, leading to abnormal follicular atresia (Shen et al., 2017). Hydrogen peroxide is commonly employed as an oxidant reagent in cell culture to induce oxidative stress (Ma et al., 2018; Zhang et al., 2021). In the present study, we evaluated the effects of H_2O_2-induced oxidative stress on autophagy in chicken

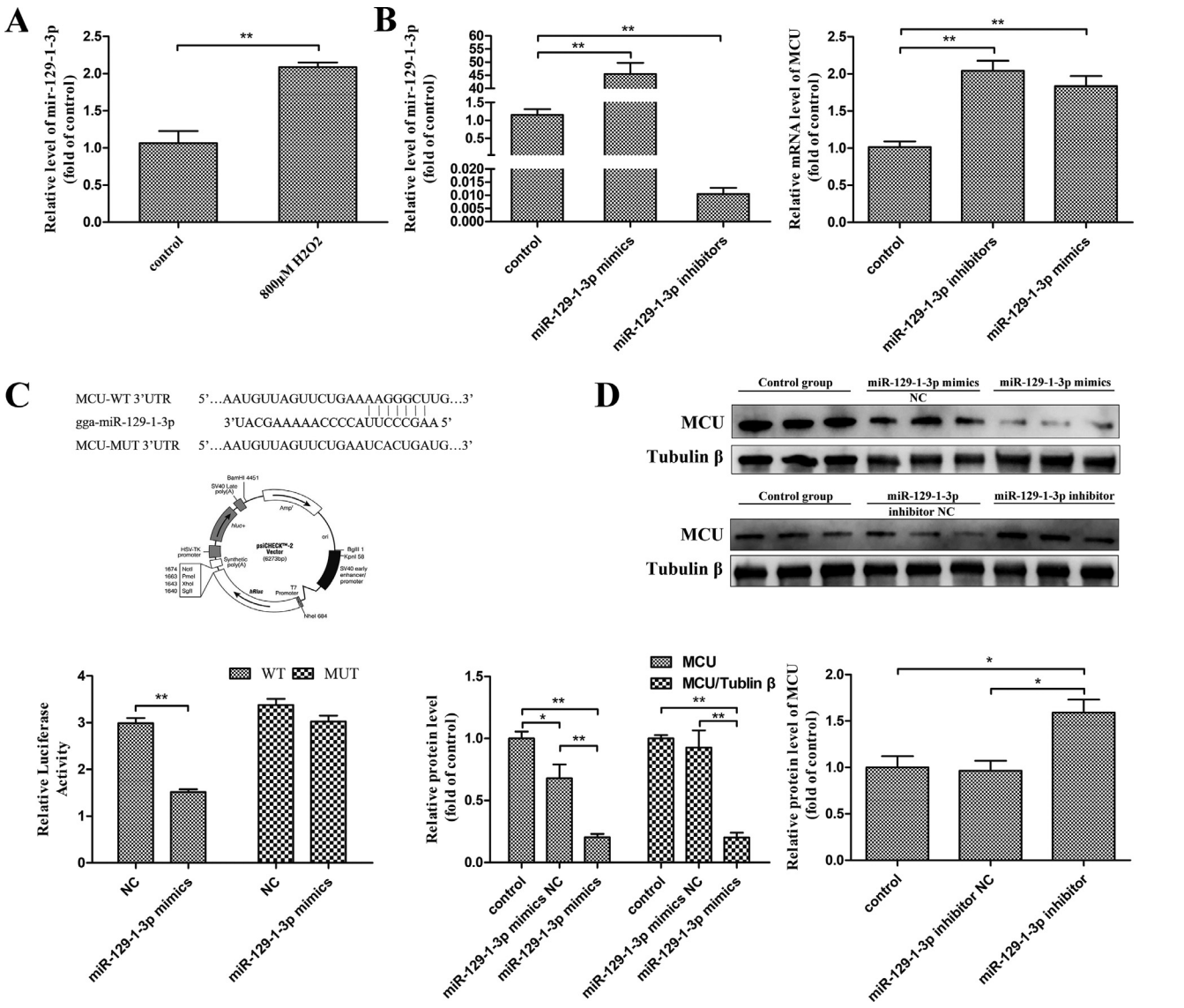

Figure 4. MiR-129-1-3p directly targets MCU. (A) Effects of H_2O_2 on the expression of miR-129-1-3p levels. (B) MCU mRNA levels in granulosa cells transfected with miR-129-1-3p mimics and inhibitor. (C) A schematic showing the 3′-untranslated regions (3′-UTRs) of the MCUs containing the wild-type or mutant miR-129-1-3p binding site, and a diagram showing the data obtained with the luciferase reporter assay. (D) Protein levels of MCU in granulosa cells transfected with miR-129-1-3p mimics, mimics NC, miR-129-1-3p inhibitor and inhibitor NC. Data are expressed as mean ± standard error of the mean (SEM) ($n = 3$). Asterisks indicate significant differences ($^*P < 0.05$ and $^{**}P < 0.01$).

granulosa cells, and explored the possible mechanism for alleviating the autophagy-related cell death caused by oxidative stress in granulosa cells. First, through animal experiments, we found that H_2O_2 treatment obviously increased the ovarian ROS production, induced granulosa cell apoptosis and follicular atresia, upregulated the expressions of GRP75, VDAC1, MCU, MFF, LC3I, and LC3II genes, and downregulated expressions of PGC-1α and MFN2 genes. Second, we further used a range of H_2O_2 concentrations, spanning from a low dose of 100 μM to a high dose of 1,000 μM, which have been previously documented to elicit autophagy or apoptosis in diverse cell types (Wu et al., 2018; Zhang et al., 2021). Our findings indicated that, when the H_2O_2 concentration reached 700 μM or higher, it impeded the growth of granulosa cells in a dose-dependent manner. Furthermore, exposure to 800 μM H_2O_2 noticeably augmented the production of ROS. Generally, physiological levels of ROS are necessary for the activation of intracellular pathways resulting in folliculogenesis, oocyte maturation, and other physiological reproductive functions (Agarwal et al., 2005). However, excessive ROS generation can induce oxidative stress, mitochondrial dysfunction and autophagy (Li et al., 2015; Singh et al., 2019). In the present study, 800 μM H_2O_2 treatment resulted in the loss of MMP, downregulation of Nrf2, PGC-1α, and Fis-1 gene expression, and elevation of Keap1, SOD2, GST, GCLC, GCLM, MFF, LC3I, LC3II, bnip3, and beclin1 gene or protein expression in granulosa cells. It was further demonstrated that oxidative stress induced by hydrogen peroxide leads to autophagic death of granulosa cells and follicular atresia in ovaries of laying hens.

Multiple studies have implicated the disruption of mitochondrial calcium homeostasis as a mechanism that contributes to the damage of cells induced by oxidative

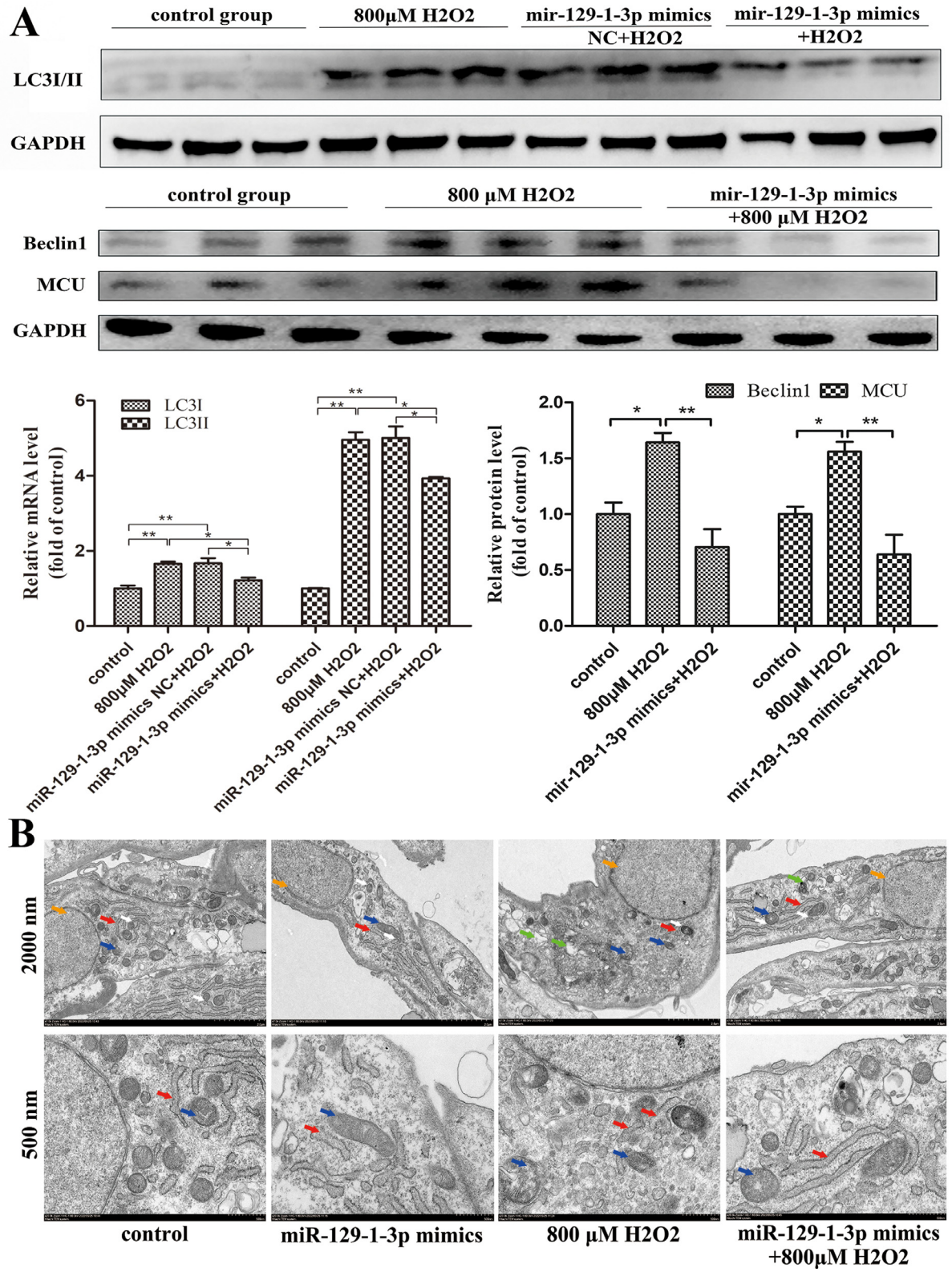

Figure 5. MIR-129-1-3p overexpression alleviates autophagy in H_2O_2-exposed granulosa cells by targeting MCU. (A) MCU and autophagy-related proteins expression. (B) Mitochondria and ER structure captured by transmission electron microscopy (orange arrowheads depict nucleus; red arrowheads depict the ER; blue arrowheads depict mitochondria; green arrowheads depict autophagosomes; white arrowheads depict ER-mitochondria contacts). Scale bars, top = 2 μm; bottom = 500 nm. Data are expressed as mean ± standard error of the mean (SEM) ($n = 3$). Asterisks indicate significant differences ($^*P < 0.05$ and $^{**}P < 0.01$).

stress (Dai et al., 2014). An excessive amount of mitochondrial calcium may trigger the opening of the mitochondrial permeability transition pore (**mPTP**), thereby exacerbating the oxidative stress (Zorov et al., 2014). Recent studies have shown that MAMs not only serve as spatial bases for the interactions between the 2 organelles, but also function as central hubs for various cellular processes, including calcium signaling,

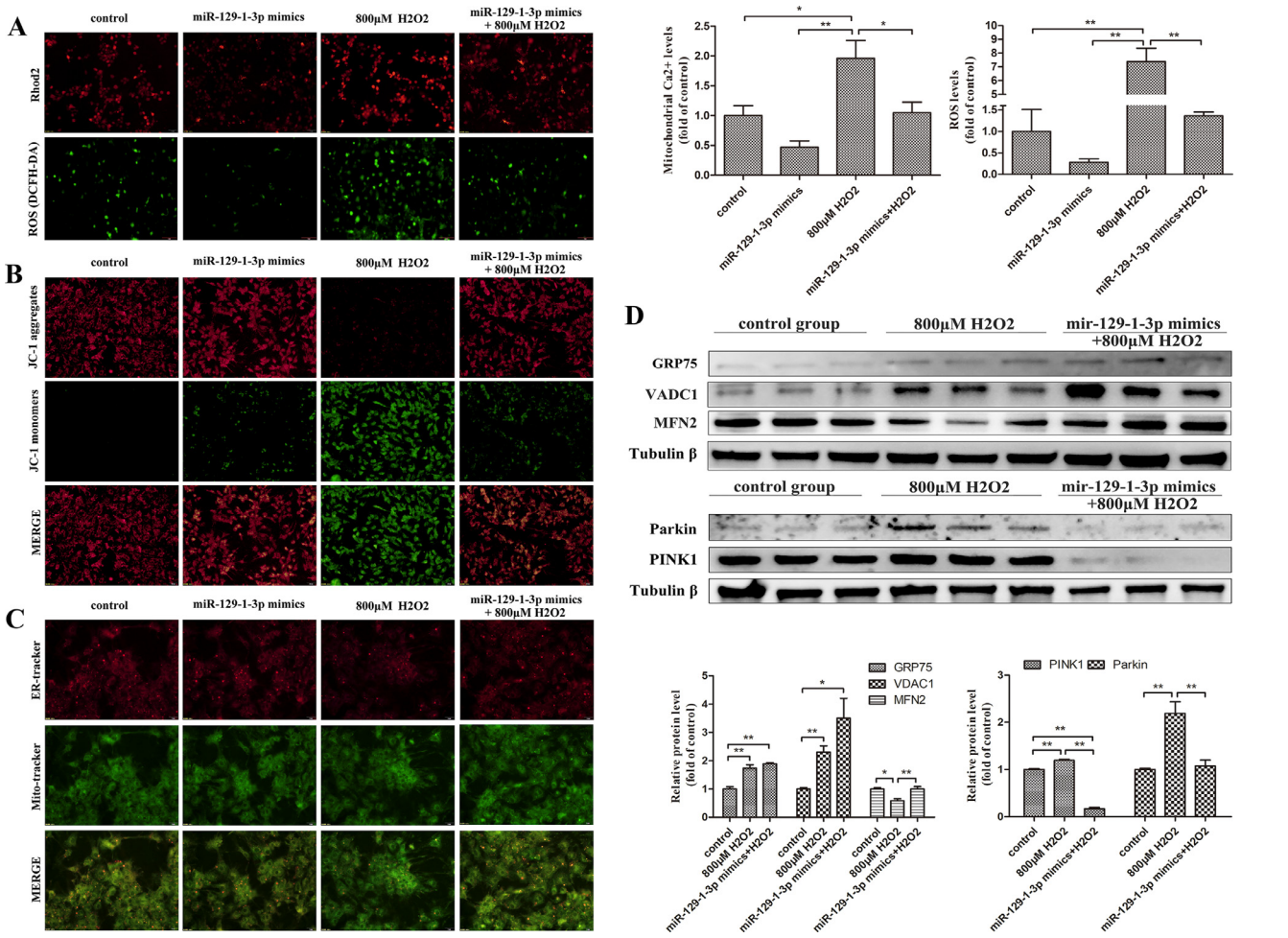

Figure 6. MiR-129-1-3p inhibits MCU decreases ROS and mitochondrial Ca^{2+} overload and improves mitochondria—ER tethering. (A) Granulosa cells stained with 2′,7′-dichlorofluorescein diacetate (DCFH-DA) and Rhod-2, and quantification of ROS and mitochondrial Ca^{2+} by DCFH-DA and Rhod-2, respectively. (B) JC-1 staining. (C) Mitochondria and ER stained with MitoTracker and ER-Tracker. (D) Mitochondria—ER tethering-related proteins expression. Data are expressed as mean ± standard error of the mean (SEM) ($n = 3$). Asterisks indicate significant differences ($^*P < 0.05$ and $^{**}P < 0.01$).

apoptosis, and autophagy (Barazzuol et al., 2021). The IP_3R-GRP75-VDAC1-MCU axis, located at MAM sites, has been shown to mediate autophagy and apoptosis by facilitating mitochondrial Ca^{2+} overload (Xu et al., 2018; Ham et al., 2020; Wang et al., 2022). In the current study, the induction of oxidative stress by H_2O_2 was found to significantly enhance the expression of IP3R, GRP75, VDAC1, and MCU genes or proteins. Additionally, treatment with H_2O_2 notably elevated the levels of mitochondrial Ca^{2+} in chicken granulosa cells. These findings imply that H_2O_2 can stimulate excessive mitochondrial Ca^{2+} accumulation via the IP3R-GRP75-VDAC1-MCU axis, consequently exacerbating oxidative stress and triggering autophagic cell death in chicken follicular granulosa cells.

Studies have shown that MCU is the final channel in the mitochondria to regulate the entry of Ca^{2+}. Therefore, cell fate can be influenced by suppressing or increasing MCU levels in order to regulate calcium signaling in cells (Liao et al., 2015; Xu et al., 2018; Cui et al., 2019). The miR-129 family is transcribed from 2 genes that share the same seed sequence "UUUUUGC": miR-129-1and miR-129-2. The miR-129-1 precursor can undergo processing to yield mature miR-129-5p and miR-129-1-3p (Li et al., 2019). Recent investigations have highlighted the pivotal role of miR-129-1-3p in the regulation of diverse biological processes, as it targets various proteins, including GRIN2D and SOX4 (Huang et al., 2020; Li et al., 2020). In the current study, we found that miR-129-1-3p, a potential biomarker of mitochondrial calcium homeostasis (Li et al., 2020, 2021), is upregulated by H_2O_2 in granulosa cell. These preliminary findings motivated us to screen the miRDB database for potential targets of miR-129-1-3p. We identified a tentative miR-129-1-3p-binding site at the 3′-UTR of MCU and confirmed that miR-129-1-3p directly regulated MCU by overexpression and knockdown of miR-129-1-3p. Furthermore, it was discovered that overexpression of miR-129-1-3p could alleviate H_2O_2-induced granulosa cell autophagy by downregulating the expression of MCU and autophagy-related proteins Beclin1, LC3I, and LC3II. These results suggest that mir-129-1-3p may attenuated oxidative stress injury of granulosa cell by inactivating MCU signal axis.

Further, we were motivated to investigate the mechanism of mir-129-1-3p alleviate oxidative stress-induced granulosa cells autophagy by targeting MCU. Numerous studies have indicated that the development of

autophagy is aggravated by Ca^{2+} retention (Bootman et al., 2018; Zhang et al., 2022). Mitochondrial matrix Ca^{2+} overload usually leads to enhanced ROS production, activation of the mPTP, depletion of ADP/ATP, and depolarization of the MMP (Brookes et al., 2004; Feissner et al., 2009). The present study showed that the overexpression of miR-129-1-3p effectively prevented mitochondrial calcium overload induced by H_2O_2, subsequently reducing cellular ROS levels and restoring MMP. The initiation of autophagosome formation is commonly recognized to occur at the MAMs location (Yang et al., 2020), which serves as the initial site for PINK/Parkin-dependent mitochondrial autophagy (Gelmetti et al., 2017; Basso et al., 2018). Mfn2, the receptor of Parkin in damaged mitochondria, is a key regulator of mitophagy downstream of Parkin (Gegg et al., 2010). During mitophagy, parkin/PINK1 rapidly phosphoubiquitinates Mfn2, leading to the dissociation of Mfn2 complexes from the outer mitochondrial membrane (**OMM**) and the separation of mitochondria from the ER (McLelland et al., 2018). Mitochondrial fusion has been reported to have beneficial effects because it enhances mitochondrial function and increases ATP production. Excessive mitochondrial fission is considered harmful due to its association with heightened mitochondrial dysfunction and ROS (Hu et al., 2019). In the present study, H_2O_2 treatment disrupts the integrity of MAMs, a phenomenon that is alleviated by the targeting of MCU by miR-129-1-3p. This intervention is accompanied by a reduction in ROS levels and the expression of Parkin and Pink1 proteins, as well as an increase in MFN2 protein expression. These results indicate that the inhibition of MCU by miR-129-1-3p hinders oxidative stress-induced mitochondrial autophagy by restoring the tethering between mitochondria and ER, and impeding the initiation of autophagy.

CONCLUSIONS

In summary, our study provides evidence that miR-129-1-3p protects H_2O_2-exposed hens' granulosa cells by decreasing the expression of MCU and subsequently mitigating mitochondrial Ca^{2+} overload, oxidative stress, MMP depolarization, mitochondrial-ER tethering damage, and mitophagy, thereby rescuing granulosa cell autophagic death. The miR-129-1-3p/MCU calcium signaling pathway may serve as a new target to alleviate follicular atresia caused by oxidative stress in laying hens.

ACKNOWLEDGMENTS

This study was supported by the earmarked fund for the National Natural Science Foundation of China (Grant No. 32202702), the Natural Science Research of Jiangsu Higher Education Institutions of China (Grant No. 22KJB230004), the Jiangsu Provincial Double-Innovation Doctor Program (Grant No. JSSCBS20211011), and the Earmarked Fund for CARS (Grant No. CARS-18).

Data Availability Statement: Data supporting this study's findings are available from the corresponding author upon reasonable request.

DISCLOSURES

No conflict of interest exits in the submission of this manuscript, and the manuscript is approved by all authors for publication. I would like to declare on behalf of my coauthors that the work described was original research that has not been published previously, and not under consideration for publication elsewhere, in whole or in part. All the authors listed have approved the manuscript that is enclosed.

REFERENCES

Agarwal, A., S. Gupta, and R. K. Sharma. 2005. Role of oxidative stress in female reproduction. Reprod. Biol. Endocrinol. 3:28.

Barazzuol, L., F. Giamogante, and T. Cali. 2021. Mitochondria associated membranes (MAMs): architecture and physiopathological role. Cell Calcium 94:102343.

Basso, V., E. Marchesan, C. Peggion, J. Chakraborty, S. von Stockum, M. Giacomello, D. Ottolini, V. Debattisti, F. Caicci, E. Tasca, V. Pegoraro, C. Angelini, A. Antonini, A. Bertoli, M. Brini, and E. Ziviani. 2018. Regulation of ER-mitochondria contacts by Parkin via Mfn2. Pharmacol. Res. 138:43–56.

Bootman, M. D., T. Chehab, G. Bultynck, J. B. Parys, and K. Rietdorf. 2018. The regulation of autophagy by calcium signals: do we have a consensus? Cell Calcium 70:32–46.

Brookes, P. S., Y. Yoon, J. L. Robotham, M. W. Anders, and S. S. Sheu. 2004. Calcium, ATP, and ROS: a mitochondrial love-hate triangle. Am. J. Physiol. Cell Physiol. 287:C817–C833.

Choi, J., M. Jo, E. Lee, and D. Choi. 2011. Induction of apoptotic cell death via accumulation of autophagosomes in rat granulosa cells. Fertil. Steril. 95:1482–1486.

Choi, J. Y., M. W. Jo, E. Y. Lee, B. K. Yoon, and D. S. Choi. 2010. The role of autophagy in follicular development and atresia in rat granulosa cells. Fertil. Steril. 93:2532–2537.

Cui, C., J. Yang, L. Fu, M. Wang, and X. Wang. 2019. Progress in understanding mitochondrial calcium uniporter complex-mediated calcium signalling: a potential target for cancer treatment. Br. J. Pharmacol. 176:1190–1205.

Dai, S. H., T. Chen, Y. H. Wang, J. Zhu, P. Luo, W. Rao, Y. F. Yang, Z. Fei, and X. F. Jiang. 2014. Sirt3 protects cortical neurons against oxidative stress via regulating mitochondrial Ca^{2+} and mitochondrial biogenesis. Int. J. Mol. Sci. 15:14591–14609.

De Stefani, D., M. Patron, and R. Rizzuto. 2015. Structure and function of the mitochondrial calcium uniporter complex. Biochim. Biophys. Acta 1853:2006–2011.

Feissner, R. F., J. Skalska, W. E. Gaum, and S. S. Sheu. 2009. Crosstalk signaling between mitochondrial Ca^{2+} and ROS. Front. Biosci. (Landmark Ed.) 14:1197–1218.

Filadi, R., P. Theurey, and P. Pizzo. 2017. The endoplasmic reticulum-mitochondria coupling in health and disease: molecules, functions and significance. Cell Calcium 62:1–15.

Gao, S. M., C. Chen, J. Wu, Y. Tan, K. Yu, C. Y. Xing, A. Ye, L. Yin, and L. Jiang. 2010. Synergistic apoptosis induction in leukemic cells by miR-15a/16-1 and arsenic trioxide. Biochem. Biophys. Res. Commun. 403:203–208.

Gegg, M. E., J. M. Cooper, K. Y. Chau, M. Rojo, A. H. Schapira, and J. W. Taanman. 2010. Mitofusin 1 and mitofusin 2 are ubiquitinated in a PINK1/parkin-dependent manner upon induction of mitophagy. Hum. Mol. Genet. 19:4861–4870.

Gelmetti, V., P. De Rosa, L. Torosantucci, E. S. Marini, A. Romagnoli, M. Di Rienzo, G. Arena, D. Vignone, G. M. Fimia, and E. M. Valente. 2017. PINK1 and BECN1 relocalize at mitochondria-associated membranes during mitophagy and promote ER-mitochondria tethering and autophagosome formation. Autophagy 13:654–669.

Ham, S. J., D. Lee, H. Yoo, K. Jun, H. Shin, and J. Chung. 2020. Decision between mitophagy and apoptosis by Parkin via VDAC1 ubiquitination. Proc. Natl. Acad. Sci. U S A 117:4281–4291.

Hu, L., M. Ding, D. Tang, E. Gao, C. Li, K. Wang, B. Qi, J. Qiu, H. Zhao, P. Chang, F. Fu, and Y. Li. 2019. Targeting mitochondrial dynamics by regulating Mfn2 for therapeutic intervention in diabetic cardiomyopathy. Theranostics 9:3687–3706.

Huang, Q., Y. S. Ou, Y. Tao, H. Yin, and P. H. Tu. 2016. Apoptosis and autophagy induced by pyropheophorbide-alpha methyl ester-mediated photodynamic therapy in human osteosarcoma MG-63 cells. Apoptosis 21:749–760.

Huang, Q., S. Xing, A. Peng, and Z. Yu. 2020,. NORAD accelerates chemo-resistance of non-small-cell lung cancer via targeting at miR-129-1-3p/SOX4 axis. Biosci. Rep. 40:BSR20193489.

Jiang, Z. F., L. Zhang, and J. Shen. 2020. MicroRNA: potential biomarker and target of therapy in acute lung injury. Hum. Exp. Toxicol. 39:1429–1442.

Jovanovic, M., and M. O. Hengartner. 2006. miRNAs and apoptosis: RNAs to die for. Oncogene 25:6176–6187.

Kim, S. G., J. Y. Sung, J. R. Kim, and H. C. Choi. 2020. Nifedipine-induced AMPK activation alleviates senescence by increasing autophagy and suppressing of Ca(2+) levels in vascular smooth muscle cells. Mech. Ageing Dev. 190:111314.

Li, P., J. Jiao, G. Gao, and B. S. Prabhakar. 2012. Control of mitochondrial activity by miRNAs. J. Cell. Biochem. 113:1104–1110.

Li, Q., M. Qin, Q. Tan, T. Li, Z. Gu, P. Huang, and L. Ren. 2020. MicroRNA-129-1-3p protects cardiomyocytes from pirarubicin-induced apoptosis by down-regulating the GRIN2D-mediated Ca(2+) signalling pathway. J. Cell. Mol. Med. 24:2260–2271.

Li, L., J. Tan, Y. Miao, P. Lei, and Q. Zhang. 2015. ROS and autophagy: interactions and molecular regulatory mechanisms. Cell. Mol. Neurobiol. 35:615–621.

Li, N., W. B. Wang, H. Bao, Q. Shi, Z. L. Jiang, Y. X. Qi, and Y. Han. 2019. MicroRNA-129-1-3p regulates cyclic stretch-induced endothelial progenitor cell differentiation by targeting Runx2. J. Cell. Biochem. 120:5256–5267.

Li, Q., D. Xu, Z. Gu, T. Li, P. Huang, and L. Ren. 2021. Rutin restrains the growth and metastasis of mouse breast cancer cells by regulating the microRNA-129-1-3p-mediated calcium signaling pathway. J. Biochem. Mol. Toxicol. 35:e22794.

Liao, Y., Y. Hao, H. Chen, Q. He, Z. Yuan, and J. Cheng. 2015. Mitochondrial calcium uniporter protein MCU is involved in oxidative stress-induced cell death. Protein Cell 6:434–442.

Ma, J., M. Li, P. K. Kalavagunta, J. Li, Q. He, Y. Zhang, O. Ahmad, H. Yin, T. Wang, and J. Shang. 2018. Protective effects of cichoric acid on H(2)O(2)-induced oxidative injury in hepatocytes and larval zebrafish models. Biomed. Pharmacother. 104:679–685.

Matsuda-Minehata, F., N. Inoue, Y. Goto, and N. Manabe. 2006. The regulation of ovarian granulosa cell death by pro- and anti-apoptotic molecules. J. Reprod. Dev. 52:695–705.

Matsuda, F., N. Inoue, N. Manabe, and S. Ohkura. 2012. Follicular growth and atresia in mammalian ovaries: regulation by survival and death of granulosa cells. J. Reprod. Dev. 58:44–50.

McLelland, G. L., T. Goiran, W. Yi, G. Dorval, C. X. Chen, N. D. Lauinger, A. I. Krahn, S. Valimehr, A. Rakovic, I. Rouiller, T. M. Durcan, J. F. Trempe, and E. A. Fon. 2018,. Mfn2 ubiquitination by PINK1/parkin gates the p97-dependent release of ER from mitochondria to drive mitophagy. Elife 7:e32866.

Michelangeli, F., O. A. Ogunbayo, and L. L. Wootton. 2005. A plethora of interacting organellar Ca^{2+} stores. Curr. Opin. Cell Biol. 17:135–140.

Peng, T. I., and M. J. Jou. 2010. Oxidative stress caused by mitochondrial calcium overload. Ann. N. Y. Acad. Sci. 1201:183–188.

Saiki, S., Y. Sasazawa, Y. Imamichi, S. Kawajiri, T. Fujimaki, I. Tanida, H. Kobayashi, F. Sato, S. Sato, K. Ishikawa, M. Imoto, and N. Hattori. 2011. Caffeine induces apoptosis by enhancement of autophagy via PI3K/Akt/mTOR/p70S6K inhibition. Autophagy 7:176–187.

Shen, M., Y. Jiang, Z. Guan, Y. Cao, L. Li, H. Liu, and S. C. Sun. 2017. Protective mechanism of FSH against oxidative damage in mouse ovarian granulosa cells by repressing autophagy. Autophagy 13:1364–1385.

Singh, A., R. Kukreti, L. Saso, and S. Kukreti. 2019,. Oxidative stress: a key modulator in neurodegenerative diseases. Molecules 24:1583.

Tai, Y., M. Pu, L. Yuan, H. Guo, J. Qiao, H. Lu, G. Wang, J. Chen, X. Qi, Z. Tao, and J. Ren. 2021. miR-34a-5p regulates PINK1-mediated mitophagy via multiple modes. Life Sci. 276:119415.

Wang, X., H. Cao, Y. Fang, H. Bai, J. Chen, C. Xing, Y. Zhuang, X. Guo, G. Hu, and F. Yang. 2022. Activation of endoplasmic reticulum-mitochondria coupling drives copper-induced autophagy in duck renal tubular epithelial cells. Ecotoxicol. Environ. Saf. 235:113438.

Wang, B., Y. Li, and C. You. 2021. miR-129-3p targeting of MCU protects against glucose fluctuation-mediated neuronal damage via a mitochondrial-dependent intrinsic apoptotic pathway. Diabetes Metab. Syndr. Obes. 14:153–163.

Wang, J. P., and K. Y. Zhang. 2021. Effects of oxidative stress on follicular atersia in poultry and its mechanism. Chin. J. Anim. Nutr. 33:3001–3009.

Wei, M. F., M. W. Chen, K. C. Chen, P. J. Lou, S. Y. Lin, S. C. Hung, M. Hsiao, C. J. Yao, and M. J. Shieh. 2014. Autophagy promotes resistance to photodynamic therapy-induced apoptosis selectively in colorectal cancer stem-like cells. Autophagy 10:1179–1192.

Wu, Z., H. Wang, S. Fang, and C. Xu. 2018. Roles of endoplasmic reticulum stress and autophagy on H_2O_2-induced oxidative stress injury in HepG2 cells. Mol. Med. Rep. 18:4163–4174.

Xing, T., X. Chen, J. Li, L. Zhang, and F. Gao. 2021,. Dietary taurine attenuates hydrogen peroxide-impaired growth performance and meat quality of broilers via modulating redox status and cell death signaling. J. Anim. Sci. 99:skab089.

Xu, H., N. Guan, Y. L. Ren, Q. J. Wei, Y. H. Tao, G. S. Yang, X. Y. Liu, D. F. Bu, Y. Zhang, and S. N. Zhu. 2018. IP(3)R-Grp75-VDAC1-MCU calcium regulation axis antagonists protect podocytes from apoptosis and decrease proteinuria in an adriamycin nephropathy rat model. BMC Nephrol. 19:140.

Yadav, A. K., P. K. Yadav, G. R. Chaudhary, M. Tiwari, A. Gupta, A. Sharma, A. N. Pandey, A. K. Pandey, and S. K. Chaube. 2019. Autophagy in hypoxic ovary. Cell. Mol. Life Sci. 76:3311–3322.

Yan, Y., X. Chen, J. Huang, C. Huan, and C. Li. 2022. H(2)O(2)-induced oxidative stress impairs meat quality by inducing apoptosis and autophagy via ROS/NF-kappaB signaling pathway in broiler thigh muscle. Poult. Sci. 101:101759.

Yang, Y., H. H. Cheung, C. Zhang, J. Wu, and W. Y. Chan. 2019. Melatonin as potential targets for delaying ovarian aging. Curr. Drug Targets 20:16–28.

Yang, M., C. Li, S. Yang, Y. Xiao, X. Xiong, W. Chen, H. Zhao, Q. Zhang, Y. Han, and L. Sun. 2020. Mitochondria-associated ER membranes - the origin site of autophagy. Front. Cell. Dev. Biol. 8:595.

Zhang, T., Q. Liu, W. Gao, S. A. Sehgal, and H. Wu. 2022. The multifaceted regulation of mitophagy by endogenous metabolites. Autophagy 18:1216–1239.

Zhang, J. Q., Q. L. Ren, J. F. Chen, B. W. Gao, X. W. Wang, Z. J. Zhang, J. Wang, Z. J. Xu, and B. S. Xing. 2021. Autophagy contributes to oxidative stress-induced apoptosis in porcine granulosa cells. Reprod. Sci. 28:2147–2160.

Zhu, M., H. Li, L. Miao, L. Li, X. Dong, and X. Zou. 2020a. Dietary cadmium chloride impairs shell biomineralization by disrupting the metabolism of the eggshell gland in laying hens. J. Anim. Sci. 98:skaa025.

Zhu, M. K., H. Y. Li, L. H. Bai, L. S. Wang, and X. T. Zou. 2020b. Histological changes, lipid metabolism, and oxidative and endoplasmic reticulum stress in the liver of laying hens exposed to cadmium concentrations. Poult. Sci. 99:3215–3228.

Zhu, M., S. Miao, W. Zhou, S. S. Elnesr, X. Dong, and X. Zou. 2021. MAPK, AKT/FoxO3a and mTOR pathways are involved in cadmium regulating the cell cycle, proliferation and apoptosis of chicken follicular granulosa cells. Ecotoxicol. Environ. Saf. 214:112091.

Zorov, D. B., M. Juhaszova, and S. J. Sollott. 2014. Mitochondrial reactive oxygen species (ROS) and ROS-induced ROS release. Physiol. Rev. 94:909–950.